HHS Public Access

Author manuscript

Oncogene. Author manuscript; available in PMC 2021 December 21.

Published in final edited form as:

Oncogene. 2021 July ; 40(29): 4809–4819. doi:10.1038/s41388-021-01907-1.

Targeting the HIF-1α-IGFBP2 axis therapeutically reduces IGF1-AKT signaling and blocks the growth and metastasis of relapsed anaplastic Wilms tumor

Yan Liu[1,*,#], **Marie V. Nelson**[2,*], **Christopher Bailey**[1], **Peng Zhang**[1], **Pan Zheng**[1,3], **Jeffrey S. Dome**[2], **Yang Liu**[1,3,#], **Yin Wang**[1,#]

[1]Division of Cancer and Immunology Research, Institute of Human Virology, University of Maryland School of Medicine, Baltimore, MD 21201

[2]Center for Cancer and Immunology Research, Children's National Hospital, Washington, DC 20010

[3]OncoC4, Inc, Rockville, MD 20852

Abstract

For patients with anaplastic Wilms tumor (WiT), metastasis and recurrence are common, and prognosis is generally poor. Novel therapies are needed to improve outcomes for patients with this high-risk WiT. A potential contributor to WiT development is constitutive activation of AKT by insulin-like growth factor 1 (IGF1) and its receptor (IGF1R) signaling pathway, but the complete underlying mechanism remains unclear. Here, we demonstrate that the hypoxia-inducible factor 1α (HIF-1α)-IGF binding protein 2 (IGFBP2) axis and the tumor-specific IGF1A are key players for constitutive activation of IGF1-AKT signaling leading to the tumor malignancy. HIF-1α and IGFBP2 are highly expressed in a majority of WiT patient samples. Deficiency of either HIF-1α or IGFBP2 or IGF1 in the tumor cells significantly impairs tumor growth and nearly abrogates metastasis in xenografted mice. Pharmacologic targeting of HIF-1α by echinomycin delivered via nanoliposomes can efficiently restrain growth and metastasis of patient-derived relapsed anaplastic WiT xenografts. Liposomal echinomycin is more potent and effective in inhibiting WiT growth than vincristine in an anaplastic WiT mouse model, and eliminates metastasis by suppressing HIF-1α targets and the HIF-1α-IGFBP2 axis, which governs IGF1-AKT signaling.

[#]Correspondence should be addressed to Yin Wang (ywang@ihv.umaryland.edu), Yang Liu (yangl@oncoc4.com), and Yan Liu (yanliu@ihv.umaryland.edu).

[*]Co-first authors

Authors' Contributions

Y. Liu: Conceptualization, data curation, formal analysis, supervision, investigation, methodology, writing original manuscript, and writing-review and editing. M.V. Nelson: Clinical sample collection, investigation, data curation, writing-original draft, and review and editing. C. Bailey: Investigation, data curation, methodology and review and editing. P. Zhang: bioinformatics analyses. J.S. Dome, P. Zheng: Formal analysis, supervision, writing-review and editing. Y. Liu, Y. Wang: Conceptualization, formal analysis, supervision, funding acquisition, project administration, writing-review and editing.

Conflict of Interest Disclosures: Authors disclosed no potential conflicts of interest.

Keywords

HIF-1α; IGFBP2; IGF1; Wilms tumor; Echinomycin; Molecular therapy

Introduction:

Wilms tumor (WiT) is the most common pediatric malignant renal tumor and the second most common extracranial solid tumor in children under 15 years of age, affecting 1 in 10,000 children [1]. Due to the emergence of clinical and biologic prognostic factors that enable the delivery of risk-directed therapy, the overall 5-year survival of patients with WiT exceeds 90% [2]. Despite these successes, up to 40% of patients with anaplastic (unfavorable) histology WiT will suffer recurrence, and <15% of those patients are expected to survive [3]. Current salvage treatments for refractory, relapsed, and metastatic disease include aggressive chemotherapy and radiation posing risk for late-effects such as infertility, secondary malignancy, and renal toxicity without guarantee of survival [4]. Therefore, novel targeted therapies are urgently needed to overcome both chemo-resistance and combined cytotoxicity in advanced WiT.

WiT is derived from transformed embryonic kidney progenitor cells in children at median age of 3-4 years. The insulin-like growth factor (IGF) family is comprised of two ligands (IGF1 and IGF2), two receptors (IGF1R and IGF2R), and six high-affinity IGF binding proteins (IGFBP 1-6). Mitogenic factor, the insulin-like growth factor 2 (IGF2), is highly expressed in WiT cells and is involved in WiT tumorigenesis by a self-stimulating autocrine loop for downstream AKT and ERK activation [5-7]. Increased expression of the IGF receptor IGF1R is associated with increased risk of relapse in patients with WiT [8]. However, the role of the ligand IGF1 in the IGF family is unknown with respect to WiT malignancy. Both IGF1 and IGF2 bind to IGF1R or the hybrid IGF1R/insulin receptor (IR-A), and only IGF1 binds to the hybrid IGF1R/IR-B, to relay downstream activation of PI3K-AKT and MAPK-ERK signaling pathways [9]. IGF2R has no receptor tyrosine kinase activity and preferentially binds IGF2 thus acting as an IGF2 antagonizing receptor. Aside from their respective peri-cellular or intracellular IGF-independent functions, IGFBPs serve to inhibit or potentiate IGF activity by modulating the bioavailability of IGFs to their receptors in the presence of IGFBP proteases, which release the ligands at extracellular matrices [10-12]. While IGF1 and IGF2 share similar binding affinity to IGFBPs 1, 3, and 4, IGF1 binds IGFBPs 2, 5, and 6 with 15- to 70-fold less affinity as compared to IGF2, and IGF1 also exhibits up to 20-fold higher binding affinity to IGF1R than IGF2, which collectively leads to IGF1 having greater accessibility and potency than IGF2 for the local activation of IGF1R signaling pathway [13, 14]. The mitogenic potency of IGF1 was originally identified by its requirement for murine embryonic, fetal, and postnatal growth, and for human embryonic stem cell self-renewal, although IGF1 is expressed at much lower levels than IGF2 throughout embryonic to postnatal periods in mice[15, 16]. Increased expression of IGF1 in cancer tissues was associated with increased tumor grades or worse prognosis in prostate [17], colorectal [18], cervical [19], ovarian [20], and triple negative breast [21] cancers. Consistently, increased IGFBP2 levels were observed in the sera and/or the cancer tissues of patients with these tumors, and IGFBP2 expression also associated with tumor progression and poor survival [22-26].

Increased IGFBP2 has also been reported in WiT tissues/cells and in the sera of WiT patients [27-29]. However, it is unknown if IGF1 is expressed in WiT cells and whether IGF1 and IGFBP2 play critical roles in WiT tumor growth and metastasis.

The transcription factor, hypoxia-inducible factor 1α (HIF-1α), primarily upregulates genes involved in glycolysis, angiogenesis, metastasis, chemo-resistance, and cell survival to metabolic stress [30]. HIF-1α regulates the malignant potential of diverse cancers and glioma stem cells under physiological hypoxia [31, 32]. Even under normoxia, HIF-1α was selectively activated in mouse lymphoma and human AML cancer stem cells allowing their survival, and echinomycin, an inhibitor of HIF-1α, has a significant therapeutic effect on relapsed AML at doses that are 30-50-fold lower than what are considered maximally tolerable in humans [33, 34]. Recently, we demonstrated that a liposomal formulation of echinomycin significantly increased therapeutic efficacy and reduced toxicity, compared to traditional Cremophor-based formulation, in leukemia and breast cancer models [35, 36]. Moreover, high prevalence of accumulated HIF-1α protein was found in WiT [37, 38], but no studies have examined its potential as a novel therapeutic target in treatment of this tumor.

We hypothesized that intratumoral hypoxia, genetic alterations, and increased IGF signaling stabilize HIF-1α, which plays a key role downstream of IGF1R-AKT signaling in a feedforward fashion to promote tumor growth, progression, and metastasis in WiT. We demonstrate here that HIF-1α, accumulated in WiT, transcriptionally induces IGFBP2 to potentiate IGF1-IGF1R-AKT signaling and promote WiT malignancy, and that this pathway is targeted effectively by the HIF-1α inhibitor echinomycin delivered via nanoliposomal formulation.

Results:

HIF-1α is accumulated and transcriptionally activated in WiT Cells

HIF-1α protein expression was evaluated within WiT samples through immunofluorescent (IF) staining using an intensity score based on percentage of cells with positive nuclear staining[37]. Qualitative evaluation of a nephroblastoma tissue microarray revealed half of WiT cases (n=32) exhibited positive HIF-1α nuclear staining in ≥50% cells (score 2). Nuclear and cytoplasmic staining was noted in tissues, with heterogeneity within and between samples (Fig. 1A-B). The majority of pediatric cases exhibited positive nuclear and strong cytoplasmic staining in 10-50% of cells (score 1) (Fig. 1B). Rabbit IgG was used as a negative control to confirm the specificity of the primary rabbit HIF-1α antibody (Fig. S1 bottom panel).

On quantitative evaluation by IF and IHC staining of 9 match-paired WiTs and normal adjacent kidney tissues (NAT), HIF-1α was found to be more highly-accumulated in WiT samples while baseline expression and fewer nuclear HIF-1α-positive cells were noted within the tubules of NAT ($P<0.001$; Fig. 1 C-D).

Two patient-derived anaplastic histology WiT primary cells (designated WiT8 and WiT10), and one patient-derived favorable histology WiT cell lines (designated WiT9) were newly established for this study and employed to establish xenografts. These newly established

xenograft WiTs showed morphologies similar to the primary tumors when grown in mice or cultured at low passage numbers *in vitro* (Fig. 1E). By Western blotting, HIF-1α was found to be accumulated in the primary cells of WiT8, WiT9 and WiT10 and the known WiT49 cell line (Fig. 1F). To test HIF-1α transcriptional activity, a red fluorescent protein (RFP) reporter driven by three tandem repeats of hypoxia responsive element (HRE) of HIF-1α was introduced into primary WiT10 cells after lentiviral infection for three days. The WiT10 cells were 36% RFP+ compared to control, which were transfected with mutant-HRE RFP reporter (Fig. 1G). These results show that HIF-1α is highly accumulated and active in WiTs.

HIF-1α is essential for and Liposomal Echinomycin inhibits the growth of WiT Cells in mouse models

Utilizing a Crispr/Cas9 system, knockout (KO) of *HIF1A* in WiT49 cell line was confirmed in two WiT49 HIF-1α-KO clones, KO3 and KO5, by Western blot (Fig. 2A) followed by sequencing of the genomic PCR products (Fig. S2A). Diminished density in the KO cell lines was noted after 1 week of colony growth by violet stain of colonies compared to scrambled sg-infected polyclonal cells, hereafter called wild-type (WT) (Fig. 2B). In xenograft recipient mice, HIF-1α KO cells either formed no tumors (HIF-1α KO5), or very small tumors (HIF-1α KO3) by day 125 following tumor cell injection, whereas recipients of control cells developed local tumors with 100% incidence and reached removal criteria (Fig. 2C).

In vitro, echinomycin was toxic to WiT49 cells and prevented proliferation at relatively low concentrations (0.45 to 4.05 nM), based on cell viability assay, and our newly established WiT cell lines (WiT8, WiT9, WiT10) responded similarly to echinomycin within the same dose range (Fig. 2D). However, WiT8 and WiT10 grew faster than WiT49 in NSG mice (Fig. 2E-G compared to 2C). Recently, we demonstrated that a liposomal reformulation of echinomycin (Lipo-EM) significantly increased therapeutic efficacy and reduced toxicity in murine models of leukemia and breast cancer [35, 36]. In NSG recipients xenografted with WiT8 or WiT10 cells, Lipo-EM-treated mice exhibited significantly reduced tumor burden versus control mice (WiT8, P=0.0018; WiT10, P=0.0008) (Fig. 2E-G), with only minor reductions in body weight (Fig. S3A,B). Like WiT49, the favorable-histology WiT9 grew very slowly in the inguinal canal of NSG mice (Fig. S3C). The difference in time of growth *in vivo* between anaplastic and favorable WiT cell lines could be attributed to *TP53* mutations in WiT8 and WiT10, but not in WiT9, which were detected by directly sequencing their PCR products of regions of 100 bp intron-flanked exons. *TP53* mutations occurred in WiT8, WiT10, and WiT49 at amino acid residues Y163C, R306*, and R248Q, respectively (Fig. S4A, B, C). These mutations caused the loss of p53 transcriptional activity, as determined by a p53 activity GFP reporter (p53-TAE) in HEK293 cells co-transfected with WT or mutant p53-expressing plasmid (Fig. S4D). Together, the results demonstrate an essential role for HIF-1α in WiT growth *in vitro* and that targeting HIF-1α inhibits WiT growth, even in the context of *TP53*-inactivating mutations.

Liposomal echinomycin inhibits WiT growth and metastasis effectively than vincristine

There are no mouse models to study WiT metastasis currently. To this end, we established the WiT10 cell line from the lung metastasis of a patient with recurrent anaplastic WiT. In xenograft recipients, WiT10 grew very aggressively locally and exhibited distant metastasis to lung, liver, and kidney tissues within 3 weeks post-injection (Fig. 3). Interestingly, Lipo-EM was more effective at inhibiting local tumor growth than the clinically-equivalent dose of vincristine, which is a standard of care for WiT (45) (Fig. 3A,B). We observed a similar effect for Lipo-EM with respect to the metastasis in the lungs, liver, and kidney tissues; although both therapies clearly reduced metastasis, we observed significantly fewer metastatic nodules in the liver ($P<0.0001$) and kidneys ($P=0.0045$) of Lipo-EM-treated mice vs those that received vincristine (Fig. 3C, E, and F). Notably, the size of the nodules was also smaller in these tissues for Lipo-EM-treated mice vs the vincristine group (Fig. 3C). Moreover, while vincristine significantly inhibited lung metastasis vs vehicle ($P<0.0001$), we could not detect any lung metastasis in Lipo-EM treated mice upon histological examination (Fig. 3C and D). As the cells originated from the lung metastasis of a WiT patient, the results suggest Lipo-EM may offer more potential for the treatment of high-risk WiT patients than the standard of care, especially with respect to metastasis. Histological sections for the remaining four mice for each of the three groups are shown in Fig. S5.

IGFBP2 is a target controlled by HIF-1α in WiT Cells

To assess which targets controlled by HIF-1α underscore the mechanism of WiT growth and metastasis we observed in mice, we analyzed the RNA sequence database of TARGET (Therapeutically Applicable Research to Generate Effective Treatment) in noncancerous kidney normal adjacent tissues (NAT, normal, 6 cases), WiTs with favorable histology (FHWT, 112 cases), and diffuse anaplastic histology (DAWT, 42 cases), with focus on known HIF-1α targets involved in anaerobic glycolysis, angiogenesis, metastasis as well as its putative targets involved in the IGF signaling pathway [39]. We found that IGFBP2 transcripts in FHWT and DAWT were higher than NAT control, although the trend did not reach statistical significance, possibly due to the small sample size of NAT (Fig. 4A). Regardless, among the 6 members of the IGF binding protein family expressed in WiT tissues, only IGFBP2 was relatively elevated vs NAT, whereas the remaining 5 members were reduced (Fig. 4A, Fig. S6).

With respect to known HIF-1α targets, expression of phosphoglycerate kinase 1 (PGK1), which plays an essential role in the aerobic glycolysis pathway, was significantly higher in DAWT vs FHWT; pyruvate dehydrogenase kinase 1 (PDK1), hexokinase 2 (HK2) and monocarboxylate transporter 1 (MCT1, encoded by *SLC16A1*), which are HIF-1α targets and key glycolytic enzymes, were significantly higher in both FHWT and DAWT compared to normal controls, indicating a role for HIF-1α in WiT glycolysis, regardless of grade and aggressiveness (Fig. 4A, Fig. S6). For the most part, the remaining HIF-1α targets we analyzed were not significantly different between the different groups; the complete summary is shown in Fig. S6. Known HIF-1α targets, *PDK1, PGK1, SLC2A3 (*encoding GLUT3), and putative targets, *IGF1, IGF2, IGFBP2, IGF1R, IRS1 and SlC16A1*, were significantly decreased in HIF-1α KO vs WT WiT49 cells (Fig. 4B and Fig. S7A). Consistent with a previous report that IGF2 and IGFBP2 expression were decreased in

embryonic mouse fibroblast cells from HIF-1α KO mice[40], we similarly observed decreased mRNA expression of IGFBP2, PGK1 and VEGF in WiT10 and WiT8 cells from Lipo-EM-vs vehicle-treated mice (Fig. S7B, C), suggesting that echinomycin blocked HIF-1α transcriptional activity.

To define IGFBP2 as a novel target of HIF-1α, we first tested for a positive correlation between HIF-1α and IGFBP2 protein expression in a WiT tissue microarray following IF staining. Generally, we observed similar staining patterns for HIF-1α and IGFBP2 in the tissues, with >60% of WiT samples (n=64) displaying high staining intensity for both proteins (Fig. 4C-D). To determine if HIF-1α can directly activate transcription of the IGFBP2 promoter, we cloned the proximal *IGFBP2* promoter upstream of a GFP reporter and subsequently co-transfected HEK293 cells with the *IGFBP2* reporter or stable HIF-1α protein (HIF-1α-PPN) (Fig. 4E). The *IGFBP2* promoter, containing 2 HRE sequences, was clearly activated in the presence of HIF-1α-PPN as determined by fluorescence microscopy and flow cytometric quantification of GFP mean fluorescence intensity (MFI) (Fig. 4F and G, respectively). Further, ChIP assay in WiT49 cells under normoxia confirmed that HIF-1α bound directly to HRE2 (rather than HRE1) in the *IGFBP2* proximal promoter, as shown in Fig. 4E and H. Thus, *IGFBP2* is a direct HIF-1α target, and the HIF-1α-IGFBP2 axis can be active in WiT cells independent of oxygen tension.

Essential Role of HIF-1α-IGFBP2 axis in the growth and metastasis of WiT

To confirm that the HIF-1α-IGFBP2 axis plays a key role in WiT malignancy, including cell division and metastatic potential, IGFBP2 knockout WiT49 cell lines were created through employment of Crispr/Cas9 system. Western blotting and sequencing of genomic PCR products confirmed IGFBP2 expression to be absent in two clones, KO13 and KO57 (Fig. 5A and Fig. S2B). As we previously observed with KO of HIF-1α, IGFBP2 KO in WiT49 cells similarly decreased colony growth *in vitro* (Fig. 5B) and abrogated tumor outgrowth *in vivo*, compared to the corresponding WT control (Fig. 5B and C, respectively). Furthermore, HIF-1α or IGFBP2 knockdown in WiT10 cells blunted local tumor growth in xenograft recipients (Fig. 5D). With respect to metastasis, knockdown of HIF-1α eliminated metastasis to lung, liver, and kidney tissues, whereas knockdown of IGFBP2 dramatically inhibited metastasis in these tissues, compared to scrambled shRNA control (Sr-sh) (Fig. 5E and F). To establish each of the targeted knockdowns, we infected the WiT-10 cells with lentivirus silencer cocktails containing an RFP reporter and two different shRNA sequences; the flow cytometry analysis of the RFP+ sorted cells given to the mice are shown in Fig. 5G and the cells were also further characterized by quantitative RT-PCR to confirm targeted knockdown (Fig. 5H). Interestingly, the RT-PCR analysis showed that knockdown of either HIF1A or IGFBP2 in isolation had a reciprocal inhibitory effect on the expression of the other gene in each case (Fig. 5H). Thus, HIF1A and IGFBP2 both regulate transcriptional expression of one another in WiT cells. Knockdown of HIF-1α or IGFBP2 in WiT10 significantly reduced the expression of HIF-1α targets and IGF signaling components (Fig.S7D). Taken together, the results demonstrate that HIF-1α and IGFBP2 activity positively correlate in an axis that is crucial for WiT growth and metastasis in the xenograft model.

IGF1A drives the growth and metastasis of WiT49 cells.

The upregulation and involvement of IGF2 in WiT tumorigenesis has been previously described [39]. However, whether IGF1 plays a role in WiT growth and metastasis is unknown. Thus, we analyzed expression of IGFs and their receptors in WiT or normal tissues using the TARGET database. As expected, IGF2 and IGF1R were expressed at significantly higher levels in either FHWT or DAWT compared to NAT controls; IGF1 levels were also elevated in either case, although not nearly as much as the former (Fig. 6A, Fig. S6A). We further examined mRNA levels of IGF1, IGF2, and IGF1R for three paired WiT samples and indicated WiT cell lines by RT-PCR, using cDNAs of mouse embryos and normal human kidney tissue as positive and negative controls, respectively. Interestingly, whereas IGF2 and IGF1R were expressed indiscriminately among cancer adjacent normal kidney and WiT tissues, we found that IGF1 mRNA expression was highly specific to WiT tissues (Fig. 6B). Since the IGF1 gene can result in three different isoforms (IGF1A, IGF1B, and IGF1C), which all produce the same mature protein but differ only in the C-terminal length, we subsequently determined by cloning the PCR products and found the tumor specific transcript was predominantly the IGF1A isoform in each case, and in WiT8 tissue from mouse where its other isoforms may exist due to the primers designed to amplify for all three isoforms (Fig. 6B). Surprisingly, WiT49 released more mature IGF1 into culture medium than the fast-growing metastatic line WiT10, and echinomycin did not affect mature IGF1 release by the two lines even though it killed most of tumor cells during 48 hr treatment (Fig. 6C). Overexpression of IGF1A in WiT49 cells reduced mature IGF1 release into medium (Fig. 6C), but we did not find that it altered cell growth in normal culture conditions. These results indicate that secreted IGF1 levels determined *in vitro* cannot predict tumor growth and metastasis or response to echinomycin treatment. Although IGF1A-overexpresing WiT49 cells had reduced mature IGF1 release *in vitro*, the cells showed increased aggressiveness *in vivo* compared to vector control cells, with respect to local tumor growth and distant metastasis to lung, liver, and kidney tissues of mice inoculated with IGF1A-WiT49 cells via subcutaneous injection into the inguinal canal (Fig. 6D-H). A similar population of the reporter RFP, which is expressed with IGF1A as a same transcript but separated by self-cleaving peptide 2A in the IGF1A- and vector control (V)-WiT49 cells sorted after lentiviral infection, was given to mice (Fig. 6D). Thus, over-expression of IGF1A detected by anti-V5 tag antibody (Fig. 6D insert) acted as mitogen driving the tumor local growth and metastasis of WiT49 cells. This IGF1A action is not surprising because pre- and mature- IGF1 both can bind to IGF1R as mitogen and the overexpression of full length of IGF1, not the mature-form IGF1, in murine muscle tissues drives muscle hypertrophy [41, 42].

To further confirm the IGF1 action *in vivo*, we knocked down IGF1 by lentiviral infection of IGF1A/RFP-WiT49 cells with IGF1 shRNA-GFP or with control Sr-shRNA-GFP, and sorted GFP-single positive cells and the RFP-GFP double positive cells in control cells, and examined the silencing efficiency by Western-blot (Fig. 6I). Knockdown of IGF1 restored the slow-growing nature of parental WiT49 in the IGF1A/RFP-WiT49 cells, while Sr-sh control RFP-GFP positive cells preserved the features of enhanced aggressiveness (Fig. 6J). Taken together, IGF1 is exclusively expressed in WiT cells and acts a potent mitogen driving the growth and metastasis of WiT *in vivo*.

HIF-1α modulates Its Own Expression through Feedforward Loop Involving IGFBP2 and IGF1-AKT signaling, which is targetable by echinomycin

To address how HIF-1α is accumulated at normoxia by IGF1 signaling, we stimulated serum-starved cells with IGF1 and found that it increased constitutive pS473-AKT and HIF-1α protein levels after 8-hour treatment, which was initiated from 15-min rapid activation of IGF1R by IGF1 in WT WiT49 cells. In contrast, these effects of IGF1 were dramatically reduced in both HIF-1α KO and IGFBP2 KO cells as measured by the pS473-AKT levels after 8-hour IGF1 treatment (Fig. 7A). Meanwhile, knockout of IGFBP2 reduced the IGF1-induced HIF-1α accumulation at normoxia as well (Fig. 7A), indicating that IGFBP2 feedback upregulated IGF1-AKT signaling for HIF-1α accumulation. Restoration of the expression of HIF-1α or IGFBP2 in HIF-1α KO WiT49 cells rescued the constitutive activation of AKT measured by pS473-AKT levels, as well as the enhanced cell growth (Fig. 7B,C and Fig. S8). To study whether this phenomenon could be mirrored in primary WiT cells, WiT10 cells with knockdown (KD) of HIF-1α or IGFBP2 were stimulated with IGF1 or EGF to observe the accumulation of HIF-1α and the constitutive activation of pS473-AKT. IGF1 dramatically increased HIF-1α accumulation and constitutive activation of AKT in Sr-sh WiT10 cells, while these effects of IGF1 were blunted in HIF-1α-KD and IGFBP-KD WiT10 cells (Fig. 7D). In contrast, EGF moderately increased HIF-1α accumulation in Sr-sh-WiT10 and the constitutive phosphor-ERK level were slightly increased independent of the knockdown of HIF-1α or IGFBP2 (Fig. 7D). The HIF-1α accumulation and constitutive activation of pS473-AKT in primary WiT cells WiT8 and WiT10 were inhibited by echinomycin as measured by Western blot following *in vitro* treatment with increasing concentrations of echinomycin (Fig. 7E).

In summary, the HIF-1α-IGFBP2 axis is required for the constitutive activation of IGF1-IGF1R-AKT signaling in WiT, which further enhances the HIF-1α-IGFBP2 axis in a feedforward manner; the enhancement of IGF1-AKT signaling via the HIF-1α-IGFBP2 axis is critical in promoting WiT growth and metastasis, and is thus targetable by HIF-1α inhibitor echinomycin (Fig. 7F).

Discussion:

Anaplastic, recurrent, and metastatic WiTs have the potential for poor outcomes despite currently available aggressive therapies. There is a lack of understanding of the underlying mechanisms essential for the WiT growth, progression and metastasis, as well as scarcity of effective molecular targets in this patient population. This is the first report to show that WiT expresses significantly higher levels of key glycolytic enzymes that are well-known HIF-1α targets, as compared to normal adjacent kidney tissues. Moreover, this is the first publication to describe HIF-1α as a key molecular target and reveal echinomycin as a potential monotherapy for treatment of high-risk malignant WiT. We also demonstrated that IGF1, specifically expressed by WiT cells, preferentially activates IGF1R-AKT signaling to cause HIF-1α accumulation and activation under normoxia. The accumulated and activated HIF-1α induces IGFBP2, which, in turn, feedforward enhances the IGF1-AKT signaling activation in a positively-regulated circuit supporting WiT malignancy. Thus, disrupting the

circuit via knockdown of IGF1, HIF-1α or IGFBP2 dramatically reduced tumor growth and metastasis.

The IGFBP2 feedforward action on the enhancement of IGF1-AKT signaling activation may not only be mediated by its binding to IGFs at extracellular matrices and cell surfaces because all other IGFBP members are down-regulated in WiT tissues as compared to normal adjacent kidney tissues. Through binding to integrin or heparin-mediated receptor tyrosine phosphatase, IGFBP2 modifies IGF1R activation by inhibiting tumor suppressor PTEN activity that is required for PI3K-AKT activation [11, 43-45]. The direct link between PTEN loss or inactivation and increased HIF-1α accumulation and activity via AKT activation has been identified in glioblastoma cell lines [46, 47]. The induction of IGFBP2 by basic transcriptional factor Sp1 was reported in MCF7 breast cancer cells [48], indicating that HIF-1α may not control basic transcription of IGFBP2.

Targeting the sustained, activated IGF-IGF1R signaling that leads the activation of PI3K-AKT and MAPK/ERK pathways has been proposed for WiT therapy. Strategies that have been proposed include reducing IGF bioavailability, blocking IGF1R tyrosine kinase activity, exploiting inhibitors for PI3K-AKT and/or MAPK/ERK pathways, and blocking VEGF activity/action [49, 50]. However, these strategies have been unsuccessful in isolation at treating WiT due to the complexities of the ligands and IGF receptors, the activated signaling pathways, and angiogenesis for WiT growth, survival and metastasis [12, 51]. We demonstrated that targeting HIF-1α by liposomal echinomycin effectively inhibited constitutive AKT activation, glycolytic key enzymes, growth factors and angiogenic VEGF simultaneously, with low toxicity. This may explain why liposomal echinomycin monotherapy was more effective at targeting WiT malignancy versus the clinically-used vincristine regimen in the novel WiT 10 xenograft model, which presents as a rapidly-growing local tumor with distant metastasis following subcutaneous transplantation. Although IGF2 and sustained activation of IGF1R signaling were shown to be involved in WiT growth [5-7], we showed that targeting HIF-1α down-regulated their expression, thus eliminating the need to target them individually.

Our study is also the first to evaluate the effect of echinomycin treatment on WiT *in vitro* and *in vivo*. While previous NCI trials had investigated the use of echinomycin in solid tumors without success [52], this was prior to the understanding that echinomycin competitively inhibits HIF-1α binding to hypoxia response elements in the promoters of HIF-1α target genes. We previously reported that echinomycin reformulated in nanoliposomes was significantly more effective and less toxic than cremophor-formulated echinomycin in mouse models of breast cancer and leukemia [35, 36]. Building on our prior work, the efficacy studies reported herein using xenograft WiT models provides further support for the development of nanoliposomal echinomycin to address the unmet need for safe and effective therapeutic HIF-1α inhibition in cancer, including advanced WiT with HIF-1α accumulation. More importantly, as liposomal echinomycin demonstrated promising efficacy in mouse models of anaplastic WiT with *TP53* mutations (which are more clinically challenging to treat [53, 54]), the data presented herein suggests that liposomal echinomycin may offer an effective treatment option for these patients.

Materials and Methods:

WiT Samples

Patient WiT samples, labeled WiT9 (favorable histology), WiT8 (diffuse anaplastic histology), WiT10 (recurrent metastatic progressive diffuse anaplastic histology), and three paired samples of adjacent normal kidney tissues and WiTs (labeled 18N/T, 23N/T and 34N/T) were obtained from the tissue bank at Children's National Center for Cancer and Immunology Research, with approval from Children's National Medical Center Institutional Review Board (Pro00004284). Patient-derived xenograft (PDX) Wilms Tumor Mouse Models were approved by IACUC and the ethical committee at Children's National Medical Center and University of Maryland School of Medicine. The WiT49 cell line has been well-described and reliably used in previous studies [55] and was tested and found to be mycoplasma free.

Patient-derived xenograft (PDX) WiT Mouse Models

NSG mice of the same gender, aged 6-8 weeks, were subcutaneously injected in the left inguinal canal with 1 x 10^6 primary WiT cells/mouse. Once a tumor was palpable (after roughly 7 days), the mice were treated with 250 μg/kg Lipo-EM intravenously every 2 days for a total of 5 doses. Control mice received empty liposome as vehicle. Tumor size was measured over time with calipers. For the animal studies, at least three mice per group were used to ensure adequate power to detect difference between groups. For all experiments testing animal survival, at least 5 animals were used per group. Animals were randomized into groups. All animal experiments have been performed at least twice. All animal studies were blinded and conducted under the guidelines of the Institutional Animal Care and Use Committee of the University of Maryland and the Children's National Medical Center.

Statistics

Statistical analyses were performed using GraphPad Prism 7. To determine statistical significance, P-values were calculated using Student's unpaired t-test (two tailed) for pairwise comparisons, or one-way ANOVA with Bonferonni's posttest for experiments involving multiple groups, or two-way ANOVA for tumor kinetics. A P value < 0.05 was considered statistically significant. Sample sizes were determined by power calculation or prior experience. All experiments were performed at least three times, producing similar results, and representative data are shown. The exact sample sizes, statistical methods, and number of experimental repeats are indicated in the figure legends for each experiment.

Supplementary Material

Refer to Web version on PubMed Central for supplementary material.

Acknowledgments

This study was supported by the grants from the National Institutes of Health National Cancer Institute CA171972, CA183030 (Yang Liu), and CA219150, CA227671 (Yin Wang).

References:

1. Dome JS, Liu T, Krasin M, Lott L, Shearer P, Daw NC et al. Improved survival for patients with recurrent Wilms tumor: the experience at St. Jude Children's Research Hospital. Journal of pediatric hematology/oncology 2002; 24: 192–198. [PubMed: 11990305]
2. Dome JS, Graf N, Geller JI, Fernandez CV, Mullen EA, Spreafico F et al. Advances in Wilms Tumor Treatment and Biology: Progress Through International Collaboration. Journal of clinical oncology : official journal of the American Society of Clinical Oncology 2015; 33: 2999–3007. [PubMed: 26304882]
3. Mavinkurve-Groothuis AM, van den Heuvel-Eibrink MM, Tytgat GA, van Tinteren H, Vujanic G, Pritchard-Jones KL et al. Treatment of relapsed Wilms tumour (WT) patients: experience with topotecan. A report from the SIOP Renal Tumour Study Group (RTSG). Pediatr Blood Cancer 2015; 62: 598–602. [PubMed: 25546733]
4. Sasso G, Greco N, Murino P, Sasso FS. Late toxicity in Wilms tumor patients treated with radiotherapy at 15 years of median follow-up. Journal of pediatric hematology/oncology 2010; 32: e264–267. [PubMed: 20736847]
5. Reeve AE, Eccles MR, Wilkins RJ, Bell GI, Millow LJ. Expression of insulin-like growth factor-II transcripts in Wilms' tumour. Nature 1985; 317: 258–260. [PubMed: 2995817]
6. Haselbacher GK, Irminger JC, Zapf J, Ziegler WH, Humbel RE. Insulin-like growth factor II in human adrenal pheochromocytomas and Wilms tumors: expression at the mRNA and protein level. Proceedings of the National Academy of Sciences of the United States of America 1987; 84: 1104–1106. [PubMed: 3029761]
7. Scott J, Cowell J, Robertson ME, Priestley LM, Wadey R, Hopkins B et al. Insulin-like growth factor-II gene expression in Wilms' tumour and embryonic tissues. Nature 1985; 317: 260–262. [PubMed: 2995818]
8. Bielen A, Box G, Perryman L, Bjerke L, Popov S, Jamin Y et al. Dependence of Wilms tumor cells on signaling through insulin-like growth factor 1 in an orthotopic xenograft model targetable by specific receptor inhibition. Proceedings of the National Academy of Sciences of the United States of America 2012; 109: E1267–1276. [PubMed: 22529373]
9. Brahmkhatri VP, Prasanna C, Atreya HS. Insulin-like growth factor system in cancer: novel targeted therapies. BioMed research international 2015; 2015: 538019. [PubMed: 25866791]
10. Miyamoto S, Nakamura M, Yano K, Ishii G, Hasebe T, Endoh Y et al. Matrix metalloproteinase-7 triggers the matricrine action of insulin-like growth factor-II via proteinase activity on insulin-like growth factor binding protein 2 in the extracellular matrix. Cancer science 2007; 98: 685–691. [PubMed: 17359288]
11. Shen X, Xi G, Maile LA, Wai C, Rosen CJ, Clemmons DR. Insulin-like growth factor (IGF) binding protein 2 functions coordinately with receptor protein tyrosine phosphatase beta and the IGF-I receptor to regulate IGF-I-stimulated signaling. Molecular and cellular biology 2012; 32: 4116–4130. [PubMed: 22869525]
12. Yau SW, Azar WJ, Sabin MA, Werther GA, Russo VC. IGFBP-2 - taking the lead in growth, metabolism and cancer. Journal of cell communication and signaling 2015; 9: 125–142. [PubMed: 25617050]
13. Germain-Lee EL, Janicot M, Lammers R, Ullrich A, Casella SJ. Expression of a type I insulin-like growth factor receptor with low affinity for insulin-like growth factor II. Biochem J 1992; 281 (Pt 2): 413–417. [PubMed: 1310594]
14. Roghani M, Lassarre C, Zapf J, Povoa G, Binoux M. Two insulin-like growth factor (IGF)-binding proteins are responsible for the selective affinity for IGF-II of cerebrospinal fluid binding proteins. The Journal of clinical endocrinology and metabolism 1991; 73: 658–666. [PubMed: 1714916]
15. Baker J, Liu JP, Robertson EJ, Efstratiadis A. Role of insulin-like growth factors in embryonic and postnatal growth. Cell 1993; 75: 73–82. [PubMed: 8402902]
16. Wamaitha SE, Grybel KJ, Alanis-Lobato G, Gerri C, Ogushi S, McCarthy A et al. IGF1-mediated human embryonic stem cell self-renewal recapitulates the embryonic niche. Nature communications 2020; 11: 764.

17. Sciarra A Words of wisdom. Re: Retrospective analysis of prostate cancer recurrence potential with tissue metabolomic profiles. Maxeiner A, Adkins CB, Zhang Y, et al. Prostate 2010;70:710-7. Eur Urol 2010; 58: 315. [PubMed: 20845545]
18. Shiratsuchi I, Akagi Y, Kawahara A, Kinugasa T, Romeo K, Yoshida T et al. Expression of IGF-1 and IGF-1R and their relation to clinicopathological factors in colorectal cancer. Anticancer Res 2011; 31: 2541–2545. [PubMed: 21873172]
19. Huang YF, Shen MR, Hsu KF, Cheng YM, Chou CY. Clinical implications of insulin-like growth factor 1 system in early-stage cervical cancer. British journal of cancer 2008; 99: 1096–1102. [PubMed: 18781172]
20. King ER, Zu Z, Tsang YT, Deavers MT, Malpica A, Mok SC et al. The insulin-like growth factor 1 pathway is a potential therapeutic target for low-grade serous ovarian carcinoma. Gynecol Oncol 2011; 123: 13–18. [PubMed: 21726895]
21. Rigiracciolo DC, Nohata N, Lappano R, Cirillo F, Talia M, Scordamaglia D et al. IGF-1/IGF-1R/FAK/YAP Transduction Signaling Prompts Growth Effects in Triple-Negative Breast Cancer (TNBC) Cells. Cells 2020; 9.
22. Ambrosini-Spaltro A, Farnedi A, Montironi R, Foschini MP. IGFBP2 as an immunohistochemical marker for prostatic adenocarcinoma. Appl Immunohistochem Mol Morphol 2011; 19: 318–328. [PubMed: 21304397]
23. Liou JM, Shun CT, Liang JT, Chiu HM, Chen MJ, Chen CC et al. Plasma insulin-like growth factor-binding protein-2 levels as diagnostic and prognostic biomarker of colorectal cancer. The Journal of clinical endocrinology and metabolism 2010; 95: 1717–1725. [PubMed: 20157191]
24. Kim YW, Bae SM, Kim YW, Park DC, Lee KH, Liu HB et al. Target-based molecular signature characteristics of cervical adenocarcinoma and squamous cell carcinoma. Int J Oncol 2013; 43: 539–547. [PubMed: 23707988]
25. Wang H, Rosen DG, Wang H, Fuller GN, Zhang W, Liu J. Insulin-like growth factor-binding protein 2 and 5 are differentially regulated in ovarian cancer of different histologic types. Mod Pathol 2006; 19: 1149–1156. [PubMed: 16729015]
26. Dean SJ, Perks CM, Holly JM, Bhoo-Pathy N, Looi LM, Mohammed NA et al. Loss of PTEN expression is associated with IGFBP2 expression, younger age, and late stage in triple-negative breast cancer. Am J Clin Pathol 2014; 141: 323–333. [PubMed: 24515759]
27. Vincent TS, Garvin AJ, Gramling TS, Hazen-Martin DJ, Re GG, Sens DA. Expression of insulin-like growth factor binding protein 2 (IGFBP-2) in Wilms's tumors. Pediatr Pathol 1994; 14: 723–730. [PubMed: 7526357]
28. Lu J, Tao YF, Li ZH, Cao L, Hu SY, Wang NN et al. Analyzing the gene expression profile of anaplastic histology Wilms' tumor with real-time polymerase chain reaction arrays. Cancer Cell Int 2015; 15: 44. [PubMed: 26136641]
29. Zumkeller W, Schwander J, Mitchell CD, Morrell DJ, Schofield PN, Preece MA. Insulin-like growth factor (IGF)-I, -II and IGF binding protein-2 (IGFBP-2) in the plasma of children with Wilms's tumour. Eur J Cancer 1993; 29A: 1973–1977. [PubMed: 7506560]
30. Semenza GL. Oxygen sensing, homeostasis, and disease. The New England journal of medicine 2011; 365: 537–547. [PubMed: 21830968]
31. Wigerup C, Pahlman S, Bexell D. Therapeutic targeting of hypoxia and hypoxia-inducible factors in cancer. Pharmacology & therapeutics 2016; 164: 152–169. [PubMed: 27139518]
32. Qiang L, Wu T, Zhang HW, Lu N, Hu R, Wang YJ et al. HIF-1alpha is critical for hypoxia-mediated maintenance of glioblastoma stem cells by activating Notch signaling pathway. Cell death and differentiation 2012; 19: 284–294. [PubMed: 21818118]
33. Wang Y, Liu Y, Malek SN, Zheng P, Liu Y. Targeting HIF1alpha eliminates cancer stem cells in hematological malignancies. Cell stem cell 2011; 8: 399–411. [PubMed: 21474104]
34. Newman B, Liu Y, Lee HF, Sun D, Wang Y. HSP90 inhibitor 17-AAG selectively eradicates lymphoma stem cells. Cancer research 2012; 72: 4551–4561. [PubMed: 22751135]
35. Bailey CM, Liu Y, Peng G, Zhang H, He M, Sun D et al. Liposomal formulation of HIF-1alpha inhibitor echinomycin eliminates established metastases of triple-negative breast cancer. Nanomedicine 2020; 29: 102278. [PubMed: 32738299]

36. Wang Y, Liu Y, Bailey C, Zhang H, He M, Sun D et al. Therapeutic targeting of TP53-mutated acute myeloid leukemia by inhibiting HIF-1alpha with echinomycin. Oncogene 2020; 39: 3015–3027. [PubMed: 32060420]
37. Karth J, Ferrer FA, Perlman E, Hanrahan C, Simons JW, Gearhart JP et al. Coexpression of hypoxia-inducible factor 1-alpha and vascular endothelial growth factor in Wilms' tumor. Journal of pediatric surgery 2000; 35: 1749–1753. [PubMed: 11101729]
38. Dungwa JV, Hunt LP, Ramani P. Overexpression of carbonic anhydrase and HIF-1alpha in Wilms tumours. BMC cancer 2011; 11: 390. [PubMed: 21910893]
39. Hu Q, Gao F, Tian W, Ruteshouser EC, Wang Y, Lazar A et al. Wt1 ablation and Igf2 upregulation in mice result in Wilms tumors with elevated ERK1/2 phosphorylation. The Journal of clinical investigation 2011; 121: 174–183. [PubMed: 21123950]
40. Feldser D, Agani F, Iyer NV, Pak B, Ferreira G, Semenza GL. Reciprocal positive regulation of hypoxia-inducible factor 1alpha and insulin-like growth factor 2. Cancer research 1999; 59: 3915–3918. [PubMed: 10463582]
41. Durzynska J, Philippou A, Brisson BK, Nguyen-McCarty M, Barton ER. The pro-forms of insulin-like growth factor I (IGF-I) are predominant in skeletal muscle and alter IGF-I receptor activation. Endocrinology 2013; 154: 1215–1224. [PubMed: 23407451]
42. Barton ER, DeMeo J, Lei H. The insulin-like growth factor (IGF)-I E-peptides are required for isoform-specific gene expression and muscle hypertrophy after local IGF-I production. J Appl Physiol (1985) 2010; 108: 1069–1076. [PubMed: 20133429]
43. Chen X, Zheng J, Zou Y, Song C, Hu X, Zhang CC. IGF binding protein 2 is a cell-autonomous factor supporting survival and migration of acute leukemia cells. J Hematol Oncol 2013; 6: 72. [PubMed: 24191913]
44. Perks CM, Vernon EG, Rosendahl AH, Tonge D, Holly JM. IGF-II and IGFBP-2 differentially regulate PTEN in human breast cancer cells. Oncogene 2007; 26: 5966–5972. [PubMed: 17369847]
45. Foulstone EJ, Zeng L, Perks CM, Holly JM. Insulin-like growth factor binding protein 2 (IGFBP-2) promotes growth and survival of breast epithelial cells: novel regulation of the estrogen receptor. Endocrinology 2013; 154: 1780–1793. [PubMed: 23515291]
46. Zundel W, Schindler C, Haas-Kogan D, Koong A, Kaper F, Chen E et al. Loss of PTEN facilitates HIF-1-mediated gene expression. Genes Dev 2000; 14: 391–396. [PubMed: 10691731]
47. Emerling BM, Weinberg F, Liu JL, Mak TW, Chandel NS. PTEN regulates p300-dependent hypoxia-inducible factor 1 transcriptional activity through Forkhead transcription factor 3a (FOXO3a). Proceedings of the National Academy of Sciences of the United States of America 2008; 105: 2622–2627. [PubMed: 18268343]
48. Mireuta M, Darnel A, Pollak M. IGFBP-2 expression in MCF-7 cells is regulated by the PI3K/AKT/mTOR pathway through Sp1-induced increase in transcription. Growth factors 2010; 28: 243–255. [PubMed: 20370577]
49. Chekhonin VP, Shein SA, Korchagina AA, Gurina OI. VEGF in tumor progression and targeted therapy. Curr Cancer Drug Targets 2013; 13: 423–443. [PubMed: 23167597]
50. Simpson A, Petnga W, Macaulay VM, Weyer-Czernilofsky U, Bogenrieder T. Insulin-Like Growth Factor (IGF) Pathway Targeting in Cancer: Role of the IGF Axis and Opportunities for Future Combination Studies. Target Oncol 2017; 12: 571–597. [PubMed: 28815409]
51. Hua H, Kong Q, Yin J, Zhang J, Jiang Y. Insulin-like growth factor receptor signaling in tumorigenesis and drug resistance: a challenge for cancer therapy. J Hematol Oncol 2020; 13: 64. [PubMed: 32493414]
52. Schilsky RL, Faraggi D, Korzun A, Vogelzang N, Ellerton J, Wood W et al. Phase II study of echinomycin in patients with advanced breast cancer: a report of Cancer and Leukemia Group B protocol 8641. Investigational new drugs 1991; 9: 269–272. [PubMed: 1783527]
53. Wegert J, Vokuhl C, Ziegler B, Ernestus K, Leuschner I, Furtwangler R et al. TP53 alterations in Wilms tumour represent progression events with strong intratumour heterogeneity that are closely linked but not limited to anaplasia. J Pathol Clin Res 2017; 3: 234–248. [PubMed: 29085664]
54. Geller JI. Current standards of care and future directions for "high-risk" pediatric renal tumors: Anaplastic Wilms tumor and Rhabdoid tumor. Urol Oncol 2016; 34: 50–56. [PubMed: 26612481]

55. Alami J, Williams BR, Yeger H. Derivation and characterization of a Wilms' tumour cell line, WiT 49. International journal of cancer 2003; 107: 365–374. [PubMed: 14506735]

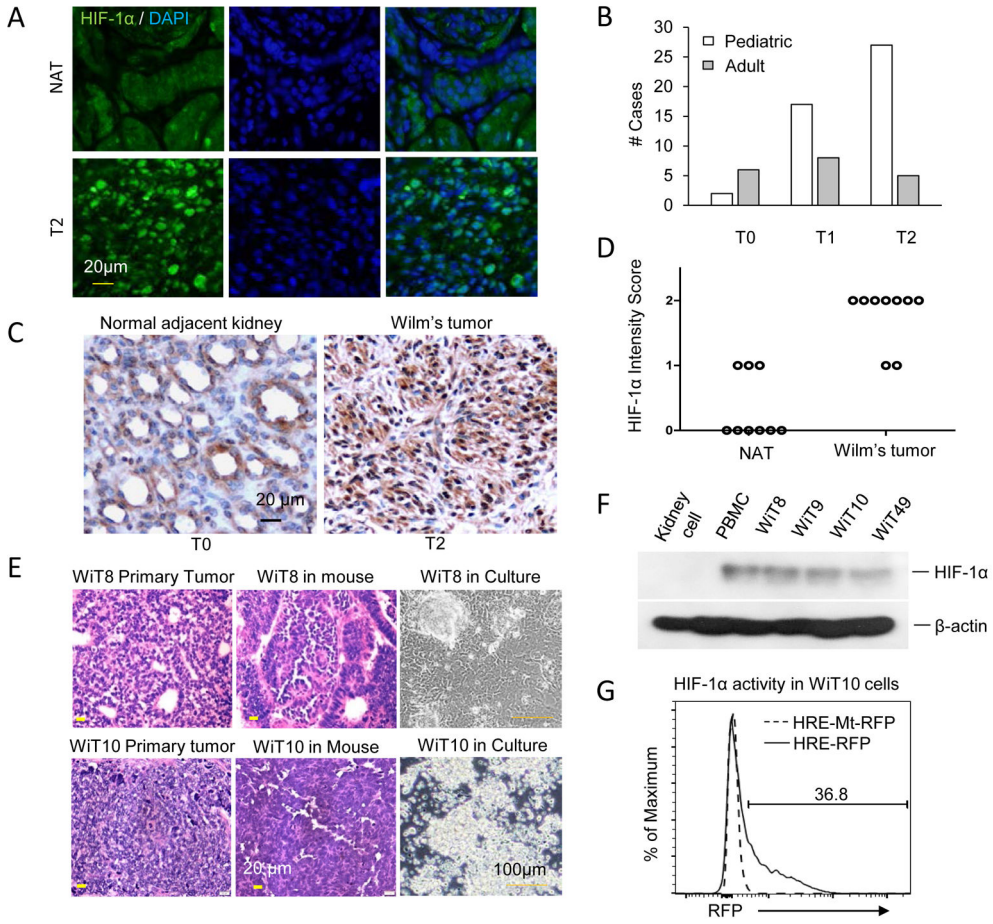

Figure 1.

HIF-1α is highly accumulated and activated in pediatric WiT. **A,** Normal kidney samples and tissue microarray including 64 WiT samples were stained for HIF-1α expression and analyzed by IF. The tissues were scored based on percent of cells with positive staining within nucleus and cytoplasm: T0 <10% cells, T1=10-50% cells, T2 >50% cells. NAT, normal adjacent kidney tissue. **B**, Distribution of WiT cases by HIF-1α intensity score (T0–2). **C,** Representative IHC staining of HIF-1α antibody in WiT9 tumor tissue depicting extensive nuclear HIF-1α staining compared with matched adjacent normal kidney tissue. **D,** Normal kidney samples WiT tissues from 9 patients were evaluated for HIF-1α expression by IF staining and scored as in (A) ($p<0.001$, paired two-tailed student's ttest). **E,** Representative images of H&E stained sections for WiT tissues, either patient derived or from the first round of transplantation in NSG recipient mice (left and middle panels, respectively), and confocal images of the respective cells in culture (first passage) after isolation from patients (right panels). **F**, Western blot of HIF-1α in murine kidney cells, human peripheral blood mononuclear cells (PBMC), primary patient-derived WiT cells (WiT8-10), and WiT cell line (WiT49). **G,** Overlayed flow cytometry histograms measuring RFP intensity in WiT10 as a readout of HIF-1α transcriptional activity. WiT10 cells were transduced with either HRE-repeat-driven RFP reporter or a mutated HRE-repeat-driven

RFP reporter as a negative control. Data shown are representative of three independent experiments.

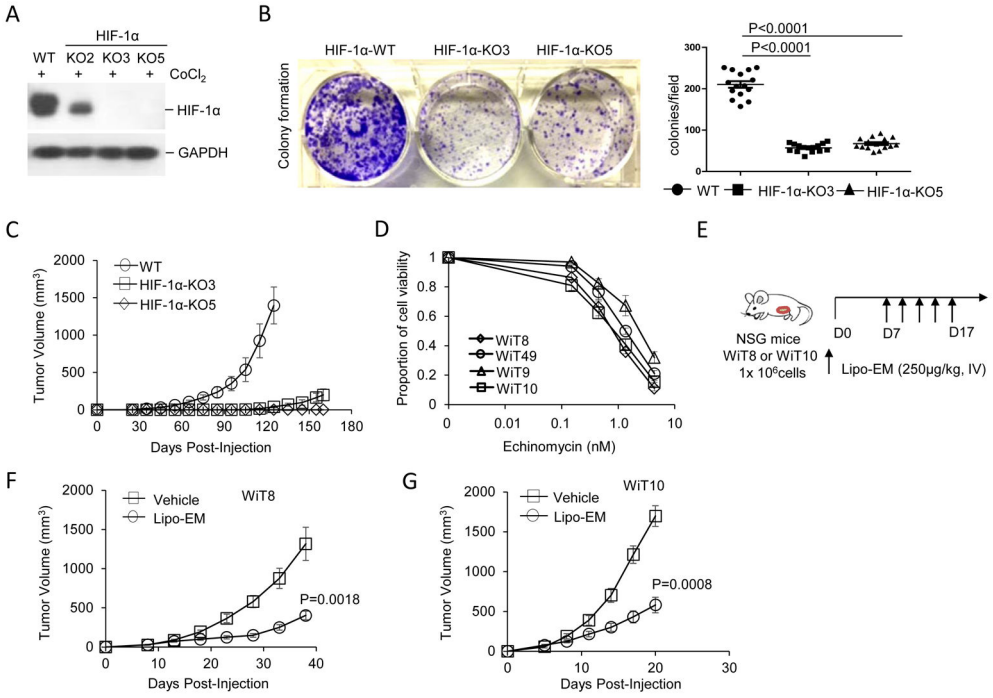

Figure 2.

HIF-1α expression is critical for WiT growth. **A,** Western blot of HIF-1α protein expression detected for WiT49 cells following editing by either Crispr-Sr-sg control (WT) or Crispr-HIF-1α-sg to generate knockout clones (KO2, KO3, and KO5) and 8 hr treatment of the cells with 350μg/ml $CoCl_2$. **B,** Photograph (left) and summarized data (right) for WiT49 colony forming ability depicting WT control vs HIF-1α-KO clones KO3 and KO5. The cells were cultured in a 6-well plate (1x 10^4 cells/well) for one week prior to applying violet stain for 15 min followed by analysis. The summarized data corresponds to number of cell colonies per view at 4X magnification from 3 different experiments (right). Data shown as mean ± SEM, and p value determined by unpaired ttest. **C,** WT or HIF-1α-KO WiT49 cells ($2x10^6$ cells/mouse) were injected into the inguinal canals of NSG mice, n=5 per group. **D,** WiT49 cells and patient-derived WiT cells were treated with increasing concentrations of echinomycin for 48 hrs and cell viability was measured by MTT assay. Data shown are representative of three independent experiments. **E,F,G**, WiT8 or WiT10 cells were injected subcutaneously into NSG mice ($1x10^6$ cells/mouse). Once tumors were palpable, mice were randomly divided into two groups (n=10 mice/group) to receive either liposomal echinomycin (250 μg/kg) or equivalent of empty liposomes control (vehicle), once every two days for total of 5 doses. Mean tumor volumes ± SEM are plotted, p value determined by 2-way ANOVA with Bonferroni's post-test.

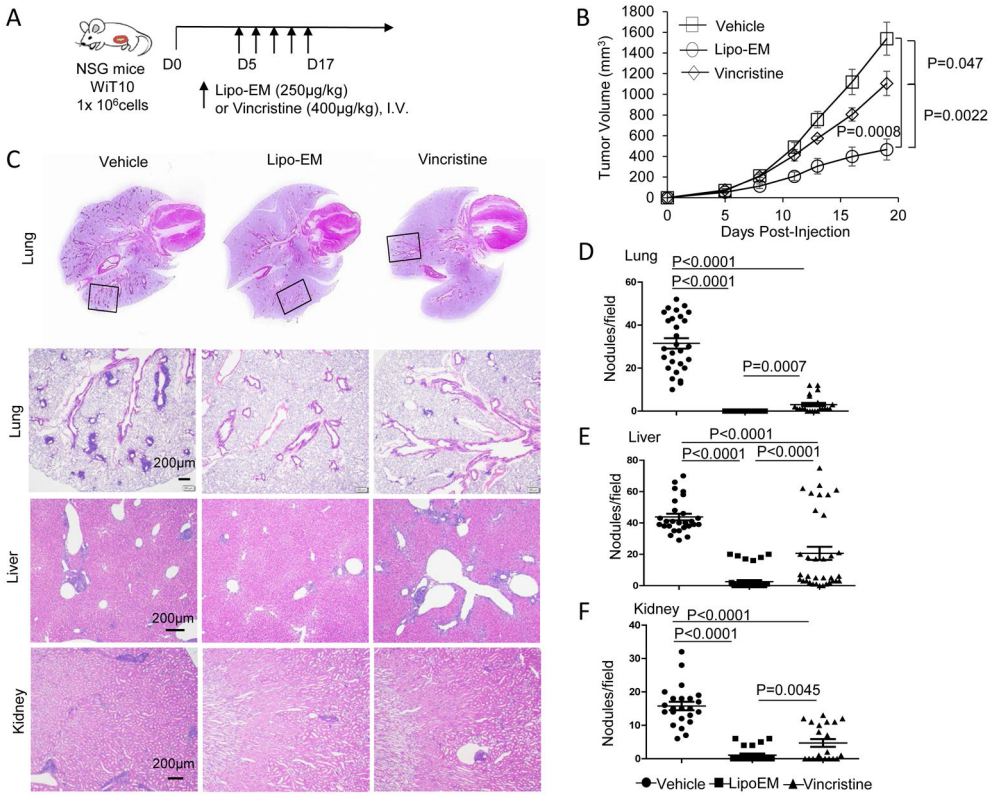

Figure 3.

Lipo-EM inhibits growth and metastasis of WiT more efficiently than vincristine. **A, B,** WiT10 cells (1x10^6 cells/mouse) were injected subcutaneously into NSG mice. Once tumors were palpable, mice were randomly grouped into 3 groups and treated with Lipo-EM (250 μg/kg, i.v.) or vincristine (400 μg/kg, i.v.), once every other 3 days for 5 doses. Local tumor volumes and mouse body weights were recorded over the course of treatment to monitor toxicity. Mean tumor volumes ± SEM are plotted, p value determined by 2-way ANOVA with Bonferroni's post-test. **C-F,** Once the size of tumors reached endpoint criteria for euthanasia, mice were perfused, and tissues were fixed in 10% formalin and sectioned. Whole lung sections from a representative mouse from each group are shown in the upper level of C, and corresponding H&E stains of lung, liver and kidney tissues are shown in the lower levels in C. Summarized data corresponding to C are shown in D, E, and F, evaluating number of metastatic nodules found in lung, liver, and kidney tissues, respectively, based on H&E staining. Data shown as mean ± SEM number of nodules per view at 10X magnification from 5 mice in each group, and p value determined by unpaired ttest. Representative of two different treatments is shown.

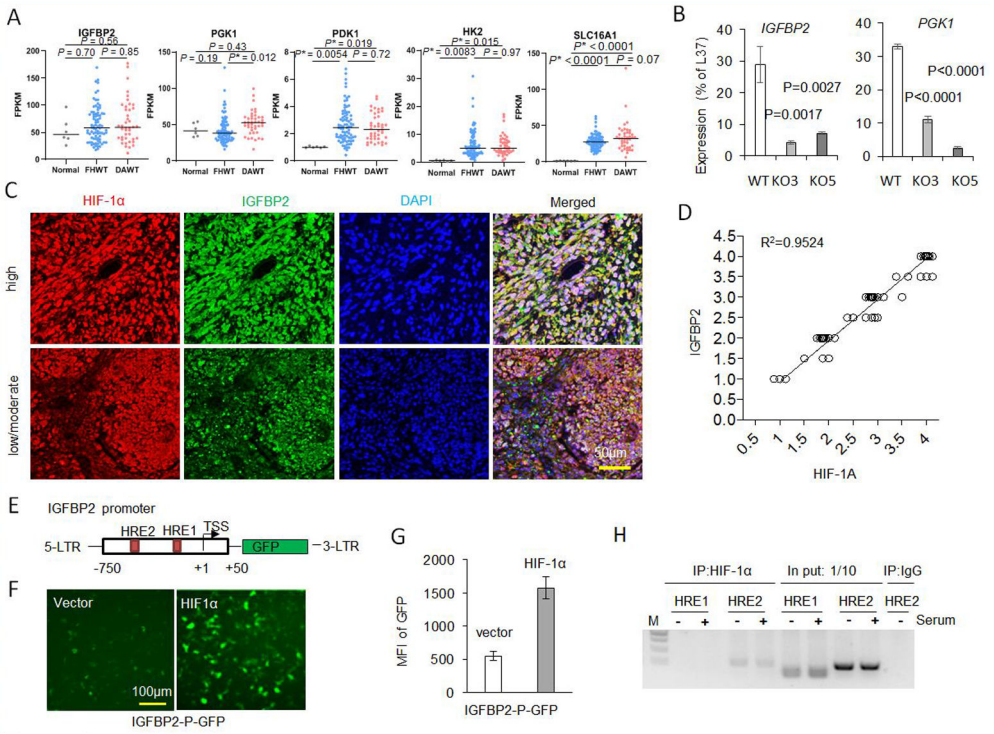

Figure 4.

IGFBP2 is a downstream target gene controlled by HIF-1α. **A,** Transcript expressions of IGFBP2 and glycolytic key enzymes in RNA-sequencing database of normal adjacent kidney tissues (NAT, 6 cases), favorable histology of WiT (FHWT, 112 cases) and diffuse anaplastic histology of WiT (DAWT, 42 cases) were analyzed. **B,** Expression of IGFBP2 and glycolytic enzyme PGK1 were decreased in HIF-1α KO WiT49 cells versus control WT cells as measured by RT-PCR. For A and B, data shown as mean ± SEM, and p value determined by unpaired ttest. **C,D,** IF staining of a 64-cases tissue microarray of WiT was performed with IGFBP2 and HIF-1α antibodies together and visualized with goat Alexa-Fluo-488 (green) and rabbit Alexa-Fluo-594 (red). The double positive stains of cases with low or moderate or high scores were analyzed for the correlation of HIF-1α with IGFBP2 (D). **E-G,** HIF-1α controls expression of IGFBP2 by binding to IGFBP2 promoter. Depiction of IGFBP2 promoter shown in E. IGFBP2 promoter-driven GFP expression in HEK293 cells, which were co-transfected with plasmids of IGFBP2 promoter plus stable HIF-1α-PPN (P402A/P564A/N803A triple mutated form) or plus empty vector for 24 hours, was photographed under microscope (F) and the mean fluorescent intensity (MFI) were measured by flow cytometry and shown after background subtraction (G). Data is shown as the mean GFP MFI ± SEM of triplicate wells Error bar represents average of triplicate wells and are representative of three independent experiments. **H,** ChIP assay was performed for WiT49 cells precipitated with anti-HIF-1α or control IgG antibodies, and PCR amplified eluted DNAs encompassing HRE sites of the IGFBP2 promoter, after the cells were deprived of serum overnight and re-stimulated with 10% FBS for 8 hrs. Data shown in F-H are representative of three independent experiments.

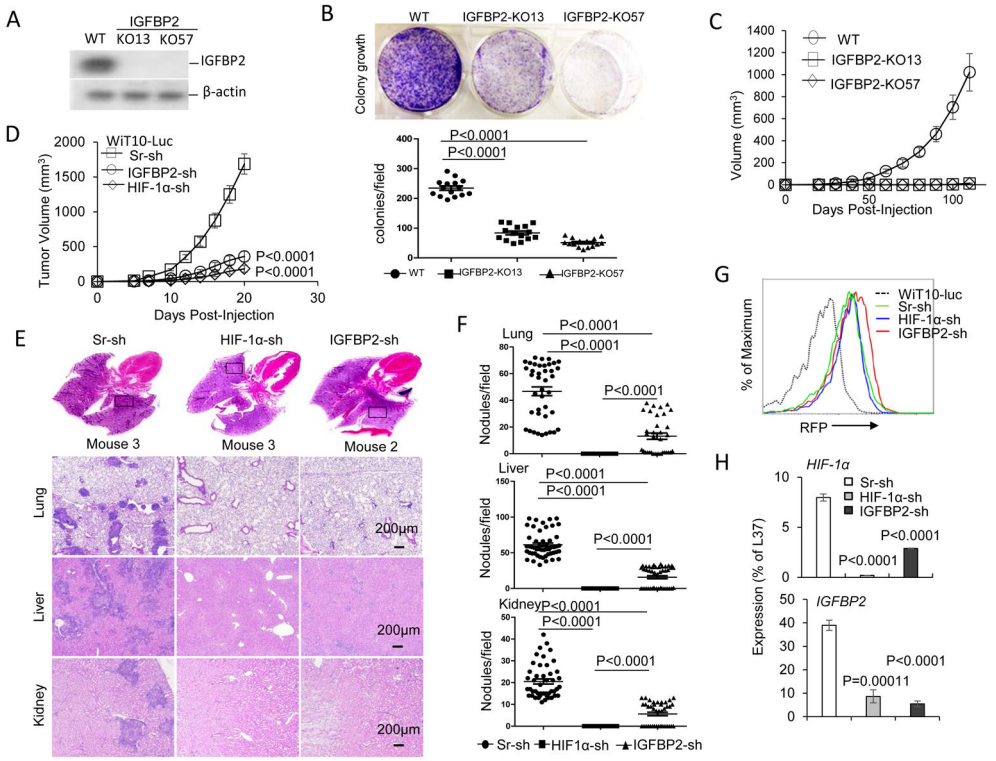

Figure 5.

HIF-1α and IGFBP2 are critical for WiT growth and metastasis. **A,** Western blot analysis depicting protein expression of IGFBP2 in Crispr-Sr-sg edited WiT49 cells (WT) and Crispr-IGFBP2-sg edited WiT49 cells with IGFBP2 knocked out (KO13 and KO57). **B,** WiT49 WT and WiT49 IGFBP2 KO lines (1x 10^4 cells/well) were cultured in a 6-well plate for 7 days and violet stain applied for 15 min to see colony formation (up panel). Summarized data corresponding to B, evaluating number of cell colonies per view at 4X magnification from 3 different experiments (below). Data shown as mean ± SEM, and p value determined by unpaired ttest. Data shown are representative of three independent experiments. **C**, WiT49 WT and WiT49 IGFBP2-KO (1 x10^6 cells/per mouse) were subcutaneously injected into 5 NSG mice of each group, and tumor growth was followed over time; mice were sacrificed at 110 days. Mean tumor volumes ± SEM are plotted, p value determined by 2-way ANOVA with Bonferroni's post-test. Data shown are representative of two independent experiments. **D, E, F,** WiT10-Luc cells expressing HIF-1α-sh-RFP (HIF-1α-sh) or IGFBP2-sh-RFP (IGFBP2-sh) or Sr-sh-RFP (Sr-sh), (1 x10^6 cells/mouse) were given subcutaneously to NSG mice, 5 mice/group (D). Mean tumor volumes ± SEM are plotted in D, with p value determined by 2-way ANOVA with Bonferroni's post-test. Once the size of tumors reached to the criteria for mouse sacrifice, mice were perfused, and tissues were fixed in 10% formalin and sectioned. Whole lung sections of representative mouse of each group were shown in the upper level of E, and the H&E stains of lung, liver and kidney tissue sections of the representative mouse were shown in the low levels in E. **F,** Summarized data corresponding to E, evaluating number of metastatic nodules found in lung, liver, and kidney tissues based on H&E staining. Data shown as mean ± SEM for number of nodules/view at 10x magnification, n=5 mice/group,

and p value determined by unpaired ttest. Representative of two different treatments is shown. **G,H,** The expression of shRNA-RFP in WiT10-Leu cells was read by flow cytometry (G) and the silencing efficiency was detected by quantitative RT-PCR (H). Data in H shown as mean ± SEM, and p value determined by unpaired ttest vs Sr-sh control.

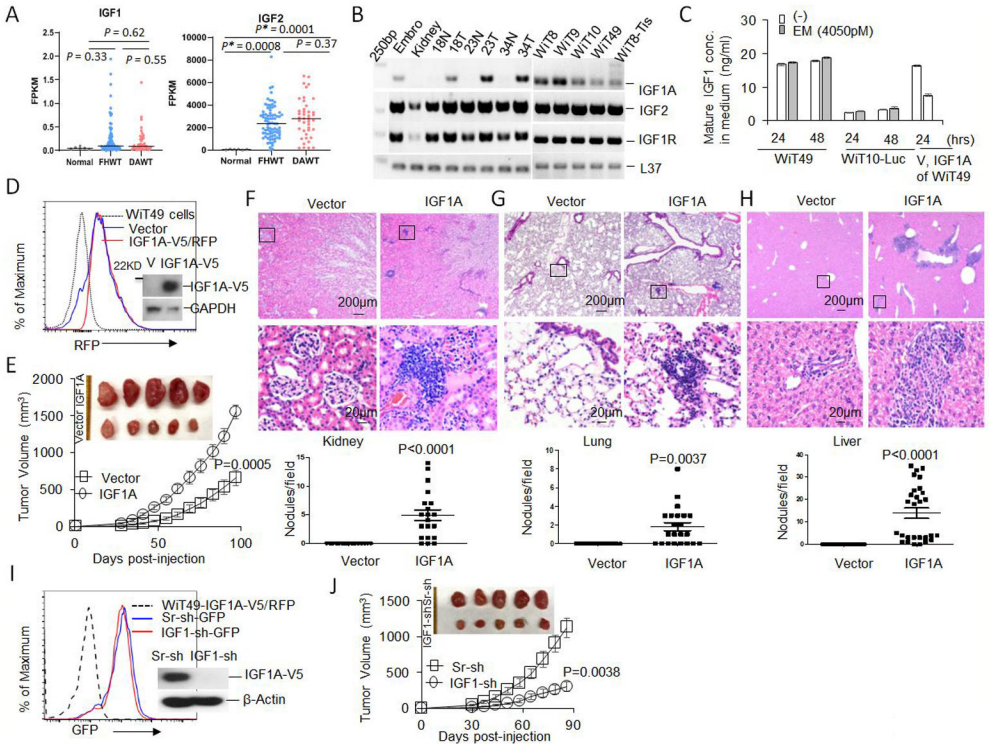

Figure 6.

IGF1 drives the growth and metastasis of WiT49 cells in vivo. **A,** Transcripts of IGF1 and IGF2 of normal adjacent kidney tissues (normal, 6 cases), favorable histology WiTs (FHWT, 112 cases) and diffuse anaplastic WiTs (DAWT, 42 cases) from RNA-Sequencing database of TARGET were analyzed. Data shown as mean ± SEM, and p value determined by unpaired ttest. **B**, RT-PCR demonstrated that IGF1A was specifically expressed in WiT tissues and cells as compared to human normal kidney tissue and the matched normal adjacent kidney tissues; the mouse embryo acts as positive control for IGF1A. **C,** ELISA detected mature IGF1 levels in the cultured medium of WiT49 and WiT10 cells treated with or without 4050 pM echinomycin for 48 hrs. **D,E,** WiT49 cells were transduced with lentivirus of IGF1A-V5/RFP or empty lenti-V5/RFP vector (V) for three days. RFP positive cells were sorted by flow-sorter (D) and IGF1A expression was examined by anti-V5 tag antibody (insert in D). One million cells/mouse of WiT49-V or WiT49-IGF1A/RFP were subcutaneously injected to 5 mice each group. Mean tumor volumes ± SEM are plotted in E, p value determined by 2-way ANOVA with Bonferroni's post-test. **F,G,H**, The mice in figure E were sacrificed on day 98 and perfused with 1XPBS. The tissues were fixed and lung, liver and kidneys were stained with H&E, and sectioned after PBS in vivo perfusion. Metastatic nodule numbers were counted as described in Fig. 5E and F, and data shown as mean ± SEM, and p value determined by unpaired ttest. **I**,**J,** WiT49-IGF1A-V5/RFP cells were transduced with lentivirus of cocktail IGF1-sh-GFP or Sr-sh-GFP for three days. GFP single positive (WiT49-IGF1-sh) and RFP-GFP double positive (WiT49-Sr-sh) (1 x10^6 cells/mouse) were subcutaneously injected to 5 mice of each group (J). Mean tumor volumes ± SEM are plotted in J, p value determined by 2-way ANOVA with Bonferroni's post-test.

Similar GFP expression in both cells was monitored by flow-cytometry but the knockdown of IGF1 was found only in WiT49-IGF1-sh cells with anti-V5 tag antibody (inserted in I).

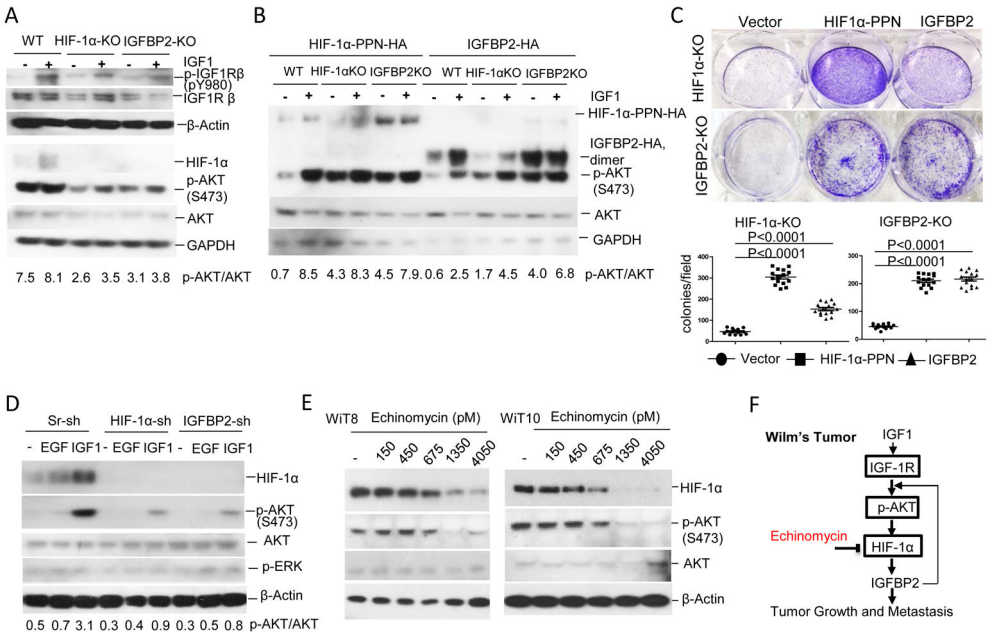

Figure 7.

HIF-1α-IGFBP2 axis enhances IGF1-IGF1R-AKT signaling for HIF-1α accumulation and feedforward regulation which are targetable by echinomycin in WiT. **A,** WiT49 WT, HIF-1α-KO (1:1 mixture of KO3 and KO5), and IGFBP2-KO (1:1 mixture of KO13 and KO57) cells were starved of serum for 8 hrs before they were stimulated with 20 ng/ml IGF1 for 15 min to detect activation of IGF1Rβ (pY980) by Western-blot. The HIF-1α and p-S473-AKT proteins were detected 8 hrs after IGF1 stimulation. **B,** Restoration of HIF-1α or IGFBP2 in their WiT49 KO cells enhances the constitutive activation of AKT compared to their control WiT49 WT cells irrespective of IGF1 stimulation. Above three lines of WiT49 cells were transiently transfected with expressing plasmid of mutated stable form of HIF-1α (HIF-1α PPN) or IGFBP2 for 24 hrs before these cells were starved of serum for 8 hrs and stimulated with 20 ng/ml IGF1 for additional 8 hrs. Western-blot detected HIF-1α and p-S473 AKT, and GAPDH as internal control. **C,** WiT49 HIF-1α KO or IGFBP2 KO cells (1 x10^4 cells/well) stably transfected with expressing plasmid of empty vector or stable HIF-1α or IGFBP2 were cultured in a 6-well plate for a week and violet stain applied for 15 min to detect colony formation (upper panel) and numbers of colonies counted under microscope from three wells were shown in bottom panel. Data shown as mean ± SEM, and p value determined by unpaired ttest. **D,** WiT10-Sr-sh, WiT10-HIF-1α-sh and WiT10 IGFBP2-sh cells were serum-starved, stimulated with 40ng/ml EGF or 20ng/ml IGF1 and detected for HIF-1α and p-S473 AKT as described in A. **E,** WiT8 and WiT10 cells were treated with increasing concentrations of free echinomycin for 48 hrs before analyzed for proteins of HIF-1α and p-S473-AKT by Western blot. Data above shown are representative of 3 independent experiments. **F,** Mechanism underlying the WiT growth and metastasis and the action of echinomycin.